European Journal of Mechanics / B Fluids 119 (2026) 204522

Contents lists available at ScienceDirect

European Journal of Mechanics / B Fluids

journal homepage: www.elsevier.com/locate/ejmflu

Generalization of a surrogate drag force model for particle laden flow

Nejc Vovk *, Jakob Kokovnik, Jure Ravnik

Faculty of Mechanical Engineering, University of Maribor, Smetanova 17, SI-2000 Maribor, Slovenia

ARTICLE INFO

Keywords:
Multiphase flow
Particle-laden flow
Particle-resolved simulation
Drag force
Surrogate models
Machine learning

ABSTRACT

We present a three-way validation of a data-driven interparticle force model against high-fidelity direct numerical simulations (DNS) and classical Faxén predictions, in the context of laminar particle-laden pipe flow. We present an Interaction-Decomposed Neural Network (IDNN) architecture, trained for unbounded flows, and perform finite-volume DNS that fully resolve the flow around stationary spherical particles placed in a circular pipe. This allows direct measurement of hydrodynamic forces for a range of particle configurations and flow conditions. Forces computed from the DNS are compared to the IDNN model evaluated on the same instantaneous geometric inputs and to analytical estimates from Faxén-type expansions. Although the IDNN was trained on unbounded flows, we show it remains predictive in pipe geometries provided the nearest walls are sufficiently distant compared with particle cloud size; in these cases the IDNN reproduces the DNS force components and trends with particle spacing and relative orientation with close quantitative agreement. The three-way comparison confirms that the IDNN can accurately reproduce resolved forces while avoiding the high cost of particle-resolved simulations and the complex Laplacian evaluations required by Faxén theory. These results inform the use of data-driven force models in Euler–Lagrange simulations and guide future model improvement for wall-influenced and strongly interacting particle systems.

1. Introduction

Particle laden flows are central to environmental transport phenomena, energy and process engineering, and biofluid systems. Simulations of dispersed particles require reliable Euler–Lagrange (EL) and/or Euler–Euler solvers and scale-bridging models for predicting hydrodynamic forces. A persistent challenge is accurate drag and, in cases when rotational dynamics is important, torque closure models across regimes that include finite particle–particle interactions, confinement, and wall proximity—conditions. These are routinely encountered in pipe flows. When such effects are ignored, simulations may mispredict pressure drop, near-wall volume fractions, dispersion, particle clustering and turbulence modulation [1].

Classical point-particle closure models are typically built from isolated-sphere correlations or from Particle-Resolved Direct Numerical Simulation (PR-DNS) of fixed assemblies, then generalized by volume fraction or Re number. Over the last decade, several advances attempted to mitigate their limitations. Pairwise interaction closures have been proposed to account for neighbour effects and improve generalization beyond dilute limits [2,3], while stochastic closures rely on mean drag with fluctuating, neighbour-induced contributions consistent with PR-DNS statistics [4]. PR-DNS simulations were also used by Xia et al. [5] to study clustering of settling suspensions. They presented a new model for the drift velocity and the variance of the solid volume fraction. The model can well predict the filtered drag and is superior to the homogeneous drag model for the clustered system. Wang et al. [6] also acknowledged that the drag force acting on a particle is vital for the accurate simulation of turbulent multiphase flows, but the robust drag model is still an open issue. They performed fully resolved direct numerical simulation with an immersed boundary method to investigate the drag force on saltating particles in wall turbulence over a sediment bed and conclude that drag models developed for an isolated particle are not suitable.

In parallel, physics-guided machine learning for force closures has emerged. Recent works use physics-informed neural networks (PINNs) to predict drag across regimes and embed constraints that enforce consistency with governing equations [7,8]. Furthermore, in contrast, research is undergoing to develop not only drag models, but data-driven deep learning models to predict the velocity, displacement, and acceleration of inertial particles in particle-laden flows [9].

It is important to distinguish between two fundamentally different hydrodynamic regimes in which closure development has progressed. At finite Re number, wake screening limits the spatial extent of hydrodynamic interactions and supports interaction models based on localized neighbour effects [3]. In contrast, in the Stokes flow

* Corresponding author.
E-mail addresses: nejc.vovk@um.si (N. Vovk), jure.ravnik@um.si (J. Ravnik).

https://doi.org/10.1016/j.euromechflu.2026.204522
Received 8 January 2026; Received in revised form 23 February 2026; Accepted 18 March 2026
Available online 20 April 2026
0997-7546/© 2026 The Authors. Published by Elsevier Masson SAS. This is an open access article under the CC BY-NC license (http://creativecommons.org/licenses/by-nc/4.0/).

limit considered here, hydrodynamic disturbances decay algebraically and remain long-ranged, rendering the drag force a manifestation of the many-body Stokes resistance operator [10]. Closure strategies developed for finite-Re conditions therefore do not directly approximate the underlying Stokesian operator governing dilute creeping-flow suspensions [11].

Confinement effects have been systematically incorporated in wall-bounded formulations, improving predictions especially in pipe and channel flows where near-wall slip and vorticity generation are dominant [12,13]. Contemporary EL studies also demonstrate the sensitivity of near-wall volume fraction and velocity statistics to the specific drag model [14].

Building on our earlier surrogate models for drag force and for interaction-driven forces in unbounded Stokesian suspensions [15,16] for an isolated particle, we seek to improve the model to consider particle clusters in unbounded flow and in wall-bounded laminar pipe flow. To achieve this we present the Interaction-Decomposed Neural Network (IDNN), a surrogate drag force model trained on a large database of PR-DNS of stationary particle clusters in unbounded Stokes flow, generated using the Boundary Element Method (BEM). Next, we examine the generalization of the model to a confined laminar pipe flow where the walls modify the local hydrodynamics. We generate a particle-resolved training database using the OpenFOAM Navier–Stokes solver, perform independent PR-DNS for stationary particle clusters placed at different wall distances in fully developed laminar pipe flow. We evaluate the surrogate model predictions against these DNS benchmarks, including a discussion of uncertainty and the applicability of Faxén-type corrections. Our results quantify how interaction-aware surrogates for Stokesian suspensions trained on unbounded configurations can transfer to wall-bounded flows, and identify conditions (geometry, placement, volume fraction) where additional physics inputs are most beneficial. Our tests were performed on finite clusters of 6 particles, additional architectures were created to predict the forces on 7–9 particles, to test the response of the particle force to an increased number of particles. The results presented herein provide a rigorous validation of the proposed framework. First, the model demonstrates quantitative agreement with established reference solutions, including direct numerical simulations (DNS) and asymptotic limits derived from Faxén-based formulations. Second, despite being trained exclusively in unbounded configurations, the model exhibits robust generalization to confined geometries. Third, the predicted responses display a systematic and physically consistent evolution as the number of interacting neighbours increases, confirming the model's sensitivity to many-body effects.

Collectively, these findings establish the reliability and physical consistency of the approach, and they constitute a necessary foundation for the development of a fully coupled, PINN-augmented N-body resistance formulation.

2. Materials and methods

This study aims to establish the generalization ability of our Interaction-Decomposed Neural Network (IDNN) surrogate model, originally trained on unbounded flow cases, when applied to confined flow environments, exemplified by laminar pipe flow. For the purpose of this research multiple numerical methods were employed: First, the Boundary Element Method (BEM) was employed to create a large database of particle-resolved simulations for the IDNN training, described in Section 2.4. Second, the Finite Volume Method (FVM) was employed in an unconventional manner to simulate multiple particle-resolved cases of stationary particles in pipe flow. In these simulations, particles were systematically positioned at varying distances from the wall. This unconventional setup was necessary to accurately capture the hydrodynamic forces arising from particle–wall and particle–particle interactions with high fidelity. The setup is presented in Section 2.1. Third, we ran inference (i.e. forward passes of the trained neural network, with the goal to obtain predictions) on the IDNN, using the same particle coordinates as they were used in the PR-DNS.

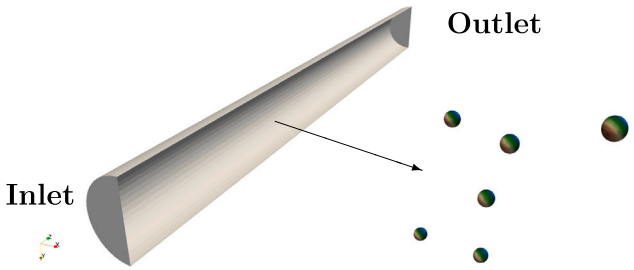


Fig. 1. Annotated pipe geometry.

2.1. The PR-DNS model

An incompressible formulation of the Navier–Stokes equation was used for physical modelling of the fluid:

$$\vec{\nabla} \cdot \vec{u} = 0, \tag{1}$$

$$\frac{\partial \vec{u}}{\partial t} + \vec{\nabla} \cdot (\vec{u} \otimes \vec{u}) = -\vec{\nabla} p + \vec{\nabla} \cdot \underline{\tau}, \tag{2}$$

where $\vec{u}$, p and $\underline{\tau}$ are the fluid velocity, kinematic pressure and stress tensor respectively. The latter is defined for laminar incompressible flows as $\vec{\nabla} \cdot \underline{\tau} = \mu \nabla^2 \vec{u}$, where μ is the fluid's dynamic viscosity, set to the value of water, $\mu = 1.004 \cdot 10^{-3}$ Pa s.

The open-source software OpenFOAM [17] was used to numerically solve the system of equations. A total of 200 cases were generated to systematically study the hydrodynamic interactions between spherical particles in a laminar flow inside a circular pipe.

The computational domain was a circular pipe with a diameter of 0.01 m and a length of 0.1 m. Each particle had a diameter of 1 μm (see Fig. 1). The particle configurations were generated such that five spherical particles were positioned randomly around a central one, according to the prescribed volume fraction $\phi = 10^{-3}$, definition of which we will define in a later section. The positions were generated using a Python routine ensuring that minimum spacing equal to the particle diameter was enforced to avoid intersections. The resulting positions were then used to create two variants of each case:

1. Full configuration: all six particles present.
2. Reduced configuration: the central particle removed and replaced by a velocity probe.

The 100 full and 100 reduced cases were obtained by progressively displacing the particle configuration from the pipe centre towards the wall in increments of 0.5 mm, reaching a maximum radial offset of 4.5 mm. In total, ten displacement positions were simulated (including the initial position at the pipe centre), and for each displacement, ten full and ten reduced cases were generated. This setup enabled the analysis of the force acting on the central particle and the disturbance velocity field at different relative positions of the neighbouring particles at the same collective radial displacement.

The velocity field was defined with a fixed uniform inlet velocity of 0.001 m/s, no-slip conditions on the pipe wall and sphere surfaces, and a $p = 0$ Pa condition at the pipe outlet.

2.2. The PR-DNS uncertainty evaluation

In order to create high fidelity PR-DNS results for critical comparison with its surrogate, the uncertainty assessment of the PR-DNS results was performed, employing the procedure by Celik et al. [18]. The uncertainty evaluation was performed for one case of a particle cloud in pipe flow with different levels of discretization around the particles, as shown in Figs. 2–4.

We monitored the total force on the particle, that is the sum of the viscous and form contribution to the drag force. Full second

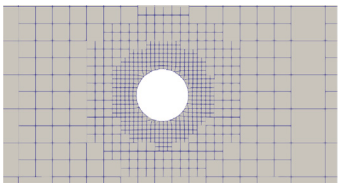


Fig. 2. Mesh with $0.7 \cdot 10^6$ global cells and 500 cells on the particle surface.

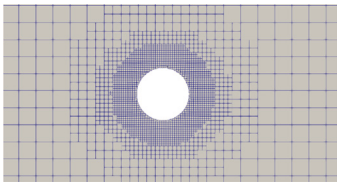


Fig. 3. Mesh with $1.4 \cdot 10^6$ global cells and 1660 cells on the particle surface.

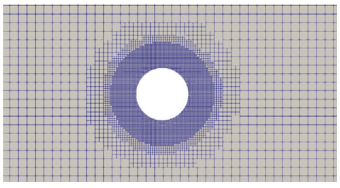


Fig. 4. Mesh with $6.6 \cdot 10^6$ global cells and 6500 cells on the particle surface.

order schemes were used for the discretization of the governing equations. We report the computed order of convergence of $p = 1.8$, the coarse-mesh numerical uncertainty $\mathrm{GCI}_{\mathrm{coarse}} = 0.6\%$ and the fine-mesh numerical uncertainty $\mathrm{GCI}_{\mathrm{fine}} = 0.2\%$. We attribute this near-theoretical convergence behaviour to the combination of (i) the smooth, well-resolved nature of the incompressible, laminar Navier–Stokes solution, and (ii) the choice of robust preconditioner settings for the pressure Poisson problem. In particular, the multigrid preconditioner used for the pressure equation yields fast and scalable convergence for Laplacian-like pressure operators. Taken together, the smooth flow physics and the multigrid-accelerated solution of the pressure equation place the numerical solution well into the asymptotic range of the discretization, which is consistent with the low GCI estimates reported above, making such approach accurate for subsequent comparison with the surrogates.

Given very low numerical uncertainty, and the fact that 10×10 simulations had to be performed, the coarse mesh (Fig. 2) was chosen for creating the PR-DNS results.

2.3. On the hydrodynamic interactions between particles in Stokes flow

Most contemporary drag closure developments have been formulated and validated in inertial or weakly inertial regimes, where hydrodynamic interactions are effectively screened by wake formation and finite-Re effects [2–6]. In such regimes, interaction effects are predominantly local, and closure strategies can be constructed around screened pairwise corrections or statistically averaged drag laws. The present work, however, addresses the Stokes flow limit, in which hydrodynamic disturbances are intrinsically long-ranged. In this regime, the force on each particle is not a local correction to an isolated drag law, but a global consequence of the many-body Stokes resistance operator.

The theoretical foundations of Stokesian dynamics are well established in the works of Brady [19], Felderhof [20], and Mazur and van Sarloos [21]. In the Stokes limit ($\mathrm{Re} \ll 1$), the inertial terms of the Navier–Stokes equations become negligible, and the fluid motion is governed by the steady, linear Stokes equations:

$$-\vec{\nabla} p^* + \mu \nabla^2 \vec{u} = 0, \quad \vec{\nabla} \cdot \vec{u} = 0, \tag{3}$$

where $p^* = p - \rho \Phi$ is written in terms of gravitational potential Φ with $\vec{g} = \vec{\nabla}\Phi$. The fundamental solution (Stokeslet), corresponding to a point force monopole $\vec{F}\delta(\vec{r})$ (e.g. microparticle) is [10]

$$\vec{u}_i = \underline{\mathrm{G}}(\vec{r}_{ij})\vec{F}_j, \tag{4}$$

where i is the observed particle at position $\vec{r}_i$ with neighbours j. Here, $\underline{\mathrm{G}}$ is the Oseen tensor (Green's function) [22],

$$\underline{\mathrm{G}}(\vec{r}_{ij}) = \frac{1}{8\pi\mu|\vec{r}_{ij}|}\left(\underline{\mathrm{I}} + \frac{\vec{r}_{ij} \otimes \vec{r}_{ij}}{|\vec{r}_{ij}|^2}\right), \quad \vec{r}_{ij} = \vec{r}_i - \vec{r}_j. \tag{5}$$

In the dilute limit, retaining only force monopoles, the linearity (Eq. (4)) generalizes to systems of multiple particles, $\vec{u}_i = \sum_{j \neq i} \underline{\mathrm{G}}_{ij}(\vec{r}_j)\vec{F}_j$, where each particle's motion induces long-range disturbances in the surrounding flow field that, in turn, affect all others [19]. This is usually defined as a mobility relation in form

$$\underline{\mathrm{u}} = \underline{\mathrm{M}}\,\underline{\mathrm{F}}, \quad \underline{\mathrm{M}}_{ii} = \frac{1}{3\pi\mu d_p}\underline{\mathrm{I}}, \quad \underline{\mathrm{M}}_{ij} = \underline{\mathrm{G}}(\vec{r}_{ij}), \tag{6}$$

where $\underline{\mathrm{u}}$ and $\underline{\mathrm{F}}$ are stacked particles' velocity and force vectors and $\underline{\mathrm{M}}$ is the so-called grand mobility matrix. For known velocities, one must solve the resistance problem as

$$\underline{\mathrm{F}} = \underline{\mathrm{R}}\,\underline{\mathrm{u}}, \quad \underline{\mathrm{R}} = \underline{\mathrm{M}}^{-1}. \tag{7}$$

Solving the full resistance formulation remains computationally demanding due to the dense, configuration-dependent nature of $\underline{\mathrm{R}}$. For small systems, direct inversion is feasible, while for larger systems, iterative approaches are typically used, often preconditioned by the block-diagonal self-resistance matrix [23]. Recent advances in Stokesian dynamics are summarized in a comprehensive review by Torre and de Graaf [24].

2.4. Surrogate model — the interaction decomposed neural network

We employ the Interaction-Decomposed Neural Network (IDNN) model (Fig. 6), which is a regression-based model that predicts the force on a particle based on its nearest neighbours, hence isolating the dependence of the force correction only on the nearest neighbours, analogously to the resistance matrix in Eq. (7). Similarly to some other authors, studying a different physical regime of dense inertial suspensions [2,25–27], we have created our training database using some form of particle-resolved DNS, in our case the Boundary Element Method (BEM). The goal of our IDNN model is to create a so-called black-box model, performing the operation

$$\vec{F}_{\mathrm{IDNN}} = f(\vec{r}_1, \ldots, \vec{r}_5), \tag{8}$$

where $\vec{F}_{\mathrm{IDNN}} \in \mathbb{R}^3$ is the drag force, predicted by the IDNN model and $\vec{r}_1, \ldots, \vec{r}_5$ are the relative coordinate vectors of five nearest neighbours, meaning f performs mapping $f : \mathbb{R}^{15} \to \mathbb{R}^3$. With a full acknowledgement of the fact that including more neighbours changes the result, we conducted preliminary tests by extending the input features of the IDNN, the results of which are presented in a later section. The initial choice of five neighbours balances capturing significant local interactions by leaning onto the fact that the off-diagonal components of the Oseen tensor (Eq. (4)) decay inversely with distance, meaning that the fifth neighbour will contribute 16% to the total interaction strength.

We chose to generate the ML database of particle coordinates and respective forces using the in-house code Andromeda [28], which employs BEM to solve the Stokes' flow governing Eqs. (3). The method is well suited for solving certain types of partial differential equations and requires only the discretization of the domain boundary Γ [29].

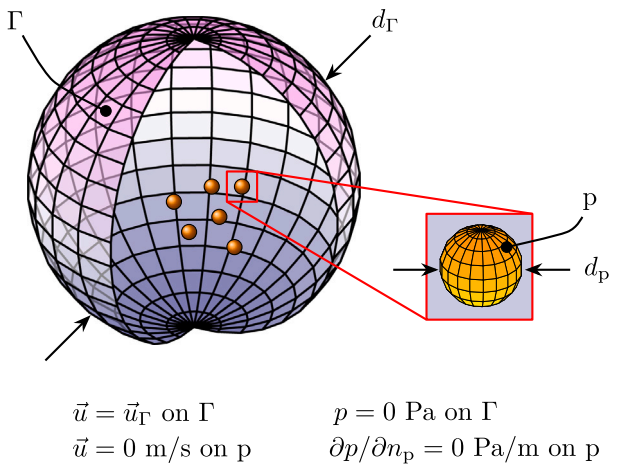


Fig. 5. Computational domain setup for the BEM simulation. The computational domain is spherical with diameter d_Γ. We put one spherical particle with size d_p in the centre of the domain, which we call the reference particle. We additionally arrange five other particles with the same size randomly around our reference particle.

The simulation setup is shown in Fig. 5. The computational domain is spherical with diameter d_Γ. We put one spherical particle with size d_p in the centre of the domain, which we call the reference particle. We additionally arrange five other particles with the same size randomly around our reference particle. A Dirichlet type boundary condition for velocity is imposed on both Γ and the particle surface p. A Dirichlet type boundary condition for pressure is also applied on Γ, and a Neumann type on p. By applying a fixed velocity $\vec{u}_\Gamma$, we simulate the so-called plug flow conditions, meaning we are able to isolate the momentum diffusion, and the inherent hydrodynamic interactions, due to the presence of particles alone. The coordinates of neighbouring particles are randomly perturbed 14 000 times to generate a particle force database of equivalent size, meaning that 14 000 BEM simulations had to be conducted. For each simulation, the volume fraction φ was estimated based on the fact, that for any Poisson-distributed set of points in 3D, the expected distance $|\vec{r}_k|$ to the kth nearest neighbour scales as [30]

$$|\vec{r}_k| \approx \left[\frac{kV_\mathrm{p}}{\alpha\varphi}\right]^{1/3}, \tag{9}$$

where α is a spatial dimension constant, which can be approximated as $4\pi/3$ in 3D and V_p is the particle volume. Arising from this, the volume fraction for the ith BEM simulation can be determined based on the distance to the fifth neighbour as

$$\varphi_i = \frac{15V_p}{4\pi|\vec{r}_5|^3}. \tag{10}$$

The size of the domain, d_Γ, is not chosen arbitrarily, as such diffusion-dominated problems are highly sensitive to the imposed boundary conditions [31]. It was found that when $d_\Gamma \approx 1024|\vec{r}_5|$, the Dirichlet pressure boundary condition, imposed on Γ, negligibly influences the particle force measurements. The calculation of the latter is trivial in BEM, as traction at the surface of the particle is obtained as a result from the solution of discretized governing equations [29], meaning that only the integration over the particle surface is needed to obtain the forces. This is unlike other methods, such as the FVM, where an extra step of numerically computing the velocity gradient is needed to obtain the shear stresses, introducing additional numerical error.

In summary, the particle force database creation procedure goes as follows:

1. A reference particle is put at the centre of the computational domain.
2. Five neighbours are added randomly around the reference particle. Here, we employ certain safety mechanisms: (i) the particles cannot overlap, (ii) the radial distance to the reference particle is limited through Eq. (10) to position our database into the bounds of $10^{-8} < \varphi < 10^{-3}$.
3. The Stokes flow solver is used to find boundary tractions at the particle surface.
4. The force on the reference particle is computed as $\vec{F}_\mathrm{d} = \int_\Gamma \vec{q}\,\mathrm{d}\Gamma$, where $\vec{q}$ is the boundary traction. The forces are stored in a nondimensional way as F/F_Stokes, where F_Stokes is the theoretical Stokes' drag force, $F_\mathrm{Stokes} = 3\pi\mu d_p|\vec{u}|$. In this description, the Stokes drag on a single particle in plug flow takes the value of $F/F_\mathrm{Stokes} = 1$.
5. The data is saved in form of a *csv* file, where each BEM simulation is represented as a row, to be later read by the regressor library. Each row has the following structure: No. of iterations, φ, F_x, F_y, F_z, r_{1x}, r_{1y}, r_{1z}, r_{2x}, r_{2y}, r_{2z}, r_{3x}, r_{3y}, r_{3z}, r_{4x}, r_{4y}, r_{4z}, r_{5x}, r_{5y}, r_{5z}. The number of iterations is monitored as a safeguard to detect and eliminate potential cases of divergence that could result in excessively high iteration counts.
6. The loop is repeated.

The IDNN architecture in Fig. 6 is motivated by the hydrodynamic interaction structure of the Stokesian dynamics formalism. In the resistance formulation, the total hydrodynamic force on a particle can be expressed as a hierarchy of many-body contributions (Eq. (7)). The IDNN explicitly decomposes the hydrodynamic force into contributions from the five nearest neighbours, sorted by their radial distance $|\vec{r}_j|$ from the reference particle. The two nearest neighbours, whose flow fields overlap most strongly, are passed jointly through the *second-order block* (blue in Fig. 6), enabling the network to represent both pairwise and three-body effects. The remaining three neighbours, which contribute predominantly through linear superposition of far-field Stokeslets, are processed individually in the *first-order block* (green), representing purely pairwise interactions. The total predicted force on the reference particle is then obtained by summing all sub-block outputs,

$$\vec{F}_\mathrm{IDNN} = \vec{F}_{12} + \vec{F}_3 + \vec{F}_4 + \vec{F}_5,$$

consistent with the linearity of Stokes flow and the superpositional structure of the grand resistance matrix.

PyTorch [32] was employed to train the IDNN. To avoid repetition, the information about the architectures is given in Appendix. Out of the entire dataset, which included 14 000 BEM simulations, 10% was reserved for validation and excluded from the training process. The model architecture, specifically the number of layers and neurons, was optimized based on the performance of the IDNN on the validation dataset using k-fold cross-validation.

This architecture thus embeds the physically justified assumption that only the closest neighbours contribute significantly to higher-order hydrodynamic interactions, while distant particles act through pairwise additive couplings. The separation of the model into streamwise and lateral components is introduced purely as a training strategy to improve convergence and predictive accuracy of the artificial neural networks. In this way, the IDNN provides a data-driven surrogate for the local resistance operator that remains faithful to the underlying hydrodynamic hierarchy.

We acknowledge that the chosen architectural partition is somewhat arbitrary and primarily serves as a proof of concept; nevertheless, allowing for third-order coupling among the two nearest neighbours is physically more consistent than neglecting such effects altogether.

Although our method does not explicitly construct the full grand resistance matrix, it can be interpreted mathematically in a similar framework. For a system of N particles, the force on particle i is

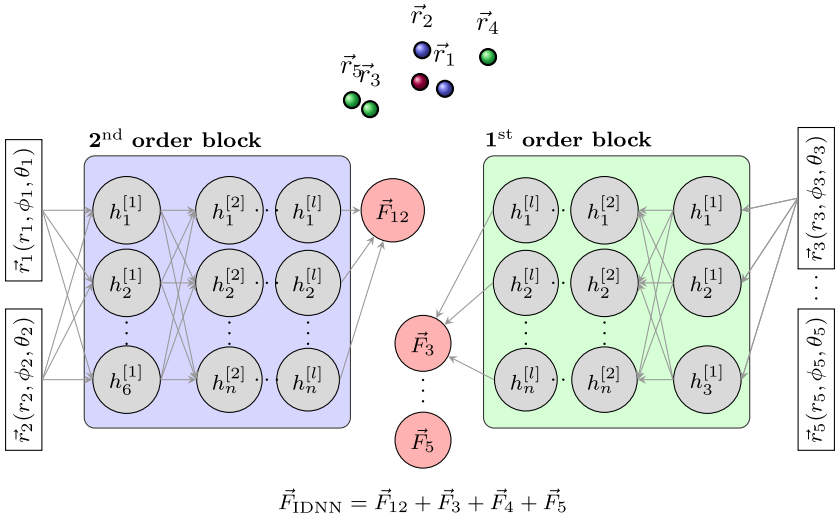


Fig. 6. Schematic representation of a single Interaction-Decomposed Neural Network (IDNN). Separate IDNNs are employed to predict the streamwise force component and the combined lateral components (spanwise and vertical). As a result, the output neuron is denoted as a vector, to indicate that it can represent either a scalar value, $\vec{F}_{IDNN} \in \mathbb{R}$, for the streamwise component, or a two-dimensional vector, $\vec{F}_{IDNN} \in \mathbb{R}^2$, for the lateral components. The IDNN features a two-block architecture, with a 1st order block for pairwise interactions and a 2nd order block for higher-order effects. For the above case, the following holds: $|\vec{r}_1| < |\vec{r}_2| < |\vec{r}_3| < |\vec{r}_4| < |\vec{r}_5|$, while the reference particle is shown in red.

approximated by summing contributions from itself and its k nearest neighbours $N_i = \{j_1, j_2, \ldots, j_k\}$:

$$\vec{F}_i \approx \vec{F}_{ii}^{\text{IDNN}} + \sum_{j \in \mathcal{N}_i} \Delta \vec{F}_{ij}^{\text{IDNN}}, \tag{11}$$

where $\vec{F}_{ij}^{\text{IDNN}}$ is the contribution from neighbour j predicted by a neural network, which takes as input the positions of surrounding particles as in Eq. (8).

We can define an implicit resistance block corresponding to each neighbour as

$$\underline{\mathrm{R}}_{ij}^{*}(\vec{r}_i, \vec{r}_j) \approx \frac{\partial \vec{F}_{ij}^{\text{IDNN}}}{\partial \vec{u}_j}, \tag{12}$$

so that the total force can be expressed in the familiar resistance-matrix form, restricted to nearest neighbours:

$$\vec{F}_i^{\text{IDNN}} \approx \underline{\mathrm{R}}_{ii}^{*} \vec{u}_i + \sum_{j \in N_i} \underline{\mathrm{R}}_{ij}^{*} \vec{u}_j. \tag{13}$$

Here, the derivative $\partial \vec{F}_{ij}^{\text{IDNN}} / \partial \vec{u}_j$ represents the local, linearized response of particle i to changes in the velocity of neighbour j, analogous to a classical resistance block in Stokes flow. This formulation allows the neural network to capture nonlinear interactions while still providing a matrix-like interpretation compatible with the familiar resistance-matrix framework.

Extending this to the entire system yields a matrix $\underline{\mathrm{R}}_{\text{IDNN}}^{*}$, where each particle interacts only with its nearest neighbours:

$$\vec{F}^{\text{IDNN}} \approx \underline{\mathrm{R}}_{\text{IDNN}}^{*} \vec{u}. \tag{14}$$

In this sense, the neural network effectively provides a data-driven approximation of the local blocks of the grand resistance matrix, bypassing the need to compute or invert the full $3N \times 3N$ matrix while capturing the dominant hydrodynamic interactions. We tested the IDNN for a cluster of six particles and compared it to Faxén theory. Additional IDNNs were trained for testing a smaller and larger number of particles, with results presented in a later section.

2.5. Faxén model

In addition to the PR-DNS and IDNN approaches to estimate the drag force on a particle in a suspension, we also consider the Faxén correction to Stokes' drag law [33]. The Faxén model estimates the hydrodynamic drag experienced by a particle immersed in a nonuniform flow field. While Stokes' expression accurately describes the drag on an isolated spherical particle in a uniform, unbounded flow, it neglects spatial variations in the surrounding velocity field. Faxén's model generalizes this by introducing higher-order corrections that account for flow curvature and gradients around the particle. Faxén showed that these effects can be expressed using the Laplacian of the velocity field, leading to an additional term that captures the curvature of the surrounding flow. The Faxén-corrected drag force is written as:

$$\vec{F}_{\text{Faxén}} = 3\pi\mu d_p \left[\left(1 + \frac{d_p^2}{24} \nabla^2 \right) \vec{u}' - (\vec{U} - \vec{u}_\infty) \right] \tag{15}$$

where $\vec{u}'$ is the disturbance of the fluid velocity at the particle's location caused by the surrounding particles, $\vec{U}$ is the particle velocity, and $\vec{u}_\infty$ is the far-field fluid velocity. The term $\frac{d_p^2}{24} \nabla^2 \vec{u}'$ represents the Faxén correction, accounting for the curvature of the flow around the particle.

The velocity disturbance $\vec{u}'$ can be estimated using analytical solutions for Stokes flow around spheres. For a system of multiple particles, the total disturbance at a given particle's location can be approximately obtained by superposing the disturbances from all other particles. In this paper, we use the PR-DNS to compute the disturbance velocity field $\vec{u}'$ at each particle's location and its Laplacian, which is then used in the Faxén formula to estimate the drag force. It is calculated using $\vec{u}' = \vec{u}_{\text{PR-DNS}} - \vec{u}_\infty$ and taking note that the velocity profile in the pipe flow is parabolic $\vec{u}_\infty = \left(u_{\max}(1 - r^2/R_{\text{pipe}}^2), 0, 0 \right)$, and as such its Laplacian is constant across the pipe cross-section: $\nabla^2 \vec{u}_\infty = \left(-4u_{\max}/R_{\text{pipe}}^2, 0, 0 \right)$.

3. Results

3.1. The IDNN training database evaluation

The BEM solver needed approximately four minutes to reach a converged solution for each particle configuration. On average, the individual simulations reached convergence in 715 ± 52 iterations of the solver of linear equations. Since our database was constructed with the goal to compute the force on a particle with respect to the coordinates of its five neighbours, the easiest way to present this data is to plot the computed force with respect to the volume fraction, calculated for each configuration with Eq. (10). The results shown in Fig. 7 show

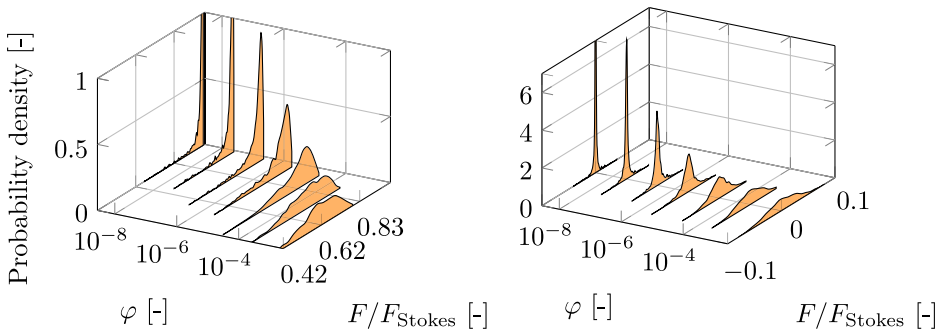


Fig. 7. Statistical evaluation of the BEM database construction results. The streamwise force (left), and the spanwise and vertical forces (right) on a reference particle F/F_{Stokes} is shown as a probability density at different particle volume fractions. The spanwise and vertical forces' probability density functions (right) are almost identical, thus they completely overlap.

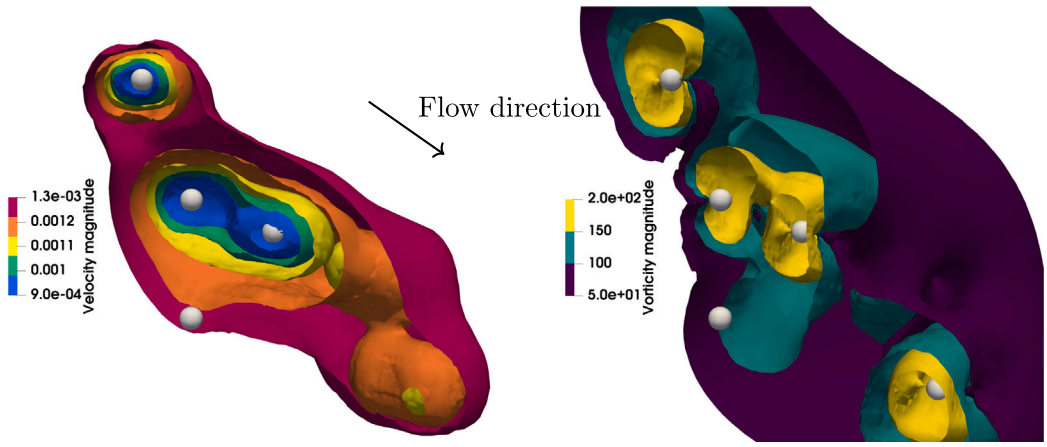


Fig. 8. The velocity magnitude contours (left) and vorticity ($\vec{\nabla} \times \vec{u}$) contours (right) visualize the flow field interactions between particles, which give rise to hydrodynamic interactions manifested as force perturbations.

that the force measurements get more dispersed with increasing volume fraction, even still deep inside the dilute regime. When we approach the dilute limit, $\varphi \to 0$, the particle becomes undisturbed by its neighbours and behaves as an isolated particle, with its kinematics governed by the Stokes drag force.

The flattening of the probability density function with increasing volume fraction suggests behaviour characteristic of a random process. However, it is important to recall that at certain volume fractions, a theoretically unlimited number of neighbour configurations is possible. For example, at $\varphi = 10^{-4}$, the streamwise drag force can vary substantially, with F/F_{Stokes} ranging from 0.9 to 0.4. Since the particle volume fraction is computed individually for each case based on the distance to the fifth nearest neighbour using Eq. (10), it assumes a homogeneous distribution of surrounding particles within this range. This assumption aligns with those made in volume-fraction-based drag force models, for a different physical regime from ours [34,35]. The proposed IDNN approach bypasses this problem by accounting for the neighbouring coordinates directly, not through the local volume fraction, making force measurements physically more accurate.

3.2. Drag force in particle cloud

Fig. 8 illustrates the flow field interactions between particles. The left panel shows the velocity magnitude contours, while the right panel presents the vorticity contours ($\vec{\nabla} \times \vec{u}$). Since the equations (Eq. (3)) are linear and elliptic, the contours exhibit smooth and symmetric structures. The absence of inertial effects eliminates downstream asymmetry and wake formation. Together, they visualize the long-range hydrodynamic coupling between particles, whereby local flow perturbations translate into hydrodynamically mediated force variations.

Fig. 9 shows the components of the hydrodynamic force, $\vec{F}$, obtained from PR-DNS, as a function of the radial displacement r/R_{pipe} of a particle cloud from the centre of a pipe. The left-hand plots depict the normalized force components, with each force component divided by the theoretical Stokes drag, $F_{\text{Stokes}} = 3\pi\mu d_p|\vec{u}|$. These normalized forces give a dimensionless representation of the forces as a function of the particle cloud's displacement. The right-hand plots show the raw values of the force components without normalization, illustrating the absolute forces acting on the particles.

The figure demonstrates how the force components, when normalized, effectively isolate the contribution from the relative particle positions, visualizing the approach used in the grand resistance matrix (Eq. (7)). This allows for a more direct comparison of the hydrodynamic interactions mediated by the fluid, focusing purely on how neighbouring particles influence one another, independent of their global position in the flow field, or their relative velocities.

3.3. The comparison of Faxén and the IDNN surrogate model drag force predictions

In the following section, we prove the adequacy of our IDNN surrogate for simulating the particle-laden pipe flow by comparing its predictions against both the high-fidelity PR-DNS results and the classical Faxén model.

In Fig. 10 we present parity plots comparing the drag force predictions from both the IDNN model and the Faxén model against the PR-DNS results. Both the IDNN model and Faxén model demonstrate good agreement with the PR-DNS data, achieving correlation coefficients above $R = 0.96$ for all three force components, while the

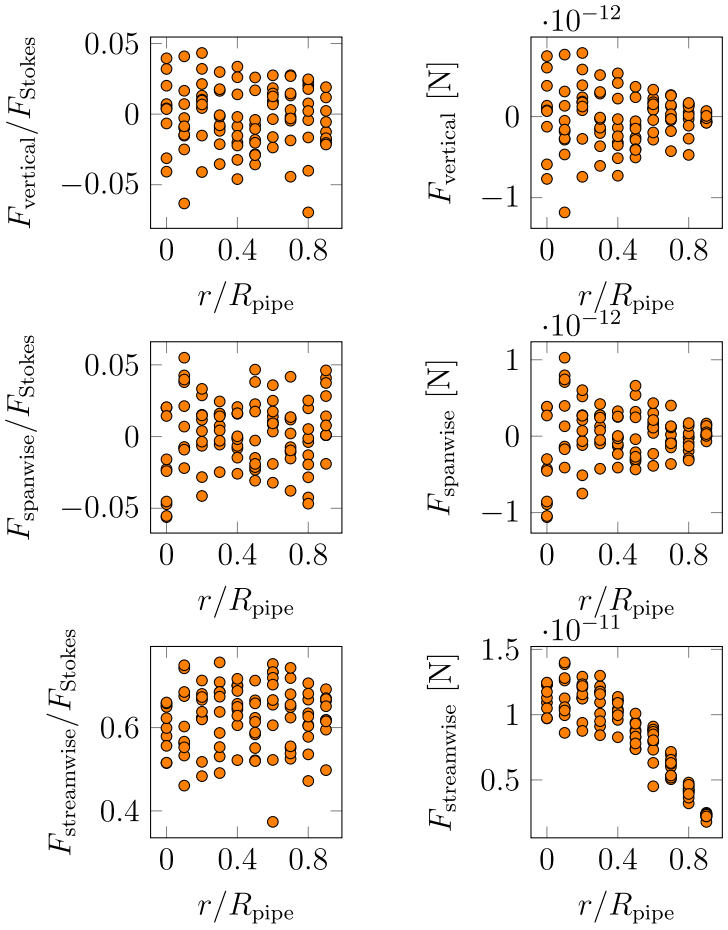


Fig. 9. Components of $\vec{F}$, obtained from PR-DNS as a function of the radial displacement in a pipe. The left column shows the normalized forces on the reference particle, thus isolating the effect of the neighbouring particles. The right column shows the same data in terms of absolute forces in order to illustrate the effect of the radial displacement.

Faxén estimates appear less accurate in terms of generalization. This indicates that while the Faxén model captures some aspects of the hydrodynamic interactions, it falls short in accurately predicting the forces experienced by particles in this complex flow environment. The error of the Faxén model is particularly pronounced in the streamwise direction when the drag force is low. This happens to be the case where the hydrodynamic interactions between particles are strongest, i.e. they are close to each other. This highlights a key limitation of the Faxén model, which does not fully account for the intricate multi-particle interactions present in such scenarios. In contrast, the IDNN model effectively captures these complex interactions, leading to good predictive performance. In Fig. 11 we present the relative error of both the IDNN model and the Faxén model with respect to the radial position in the pipe. It is evident that the IDNN model outperforms the Faxén model in all three force components, especially in the streamwise direction, where the Faxén model's error exceeds 10%. The IDNN model maintains a relative error below 5% across all radial positions, demonstrating its superior accuracy in capturing the complex hydrodynamic interactions in particle-laden pipe flow.

3.4. On the inclusion of more than five particles

The IDNN, compared to the Faxén model, incorporates hydrodynamic interactions from the five nearest neighbours. While it is acknowledged that including additional neighbours alters the predicted force, we performed preliminary sensitivity analyses by extending the input space of the IDNN to incorporate a larger number of neighbouring particles. In particular, the off-diagonal components of the Oseen tensor (Eq. (4)) decay proportionally to the inverse of the interparticle distance, implying that the fifth neighbour contributes approximately 16% relative to the leading interaction under typical spacing conditions. The respective IDNN architectures are shown in Appendix. The test was performed in the following manner: we trained separate IDNNs for each number of neighbours, $k \in 1 \dots 8$, using separate BEM databases, each consisting of $\sim 14\,000$ simulations. Next, we created a new independent database of 1000 particle clusters, each consisting of 9 particles. For each cluster, we ran inference using each of the trained IDNNs, starting with $k = 1$, accounting for only the nearest neighbour, up to $k = 8$, accounting for all neighbours. The results were then compared to the case where $k = 8$, which we consider as the reference case. The goal is to observe how the force on a particle changes as more neighbours are included in the model.

Fig. 12 shows the error and predicted force for different number of neighbours compared to the case where $k = 8$. It is evident that including more than five neighbours still consistently reduces the error, albeit with small improvements. The left panel shows that with $k = 5$, the results lie within 5% of the $k = 8$ case for almost all volume fractions. The error appears to increase with increasing volume fraction, which is expected as nonlinear effects become more pronounced, which is in line with the Oseen theory [10] for widely separated spheres.

4. Discussion and conclusions

In this work we present a surrogate drag-force model for particle laden flows. The model was trained on unbounded, low-Re Stokes DNS simulation and can generalize to wall-bounded laminar pipe flow

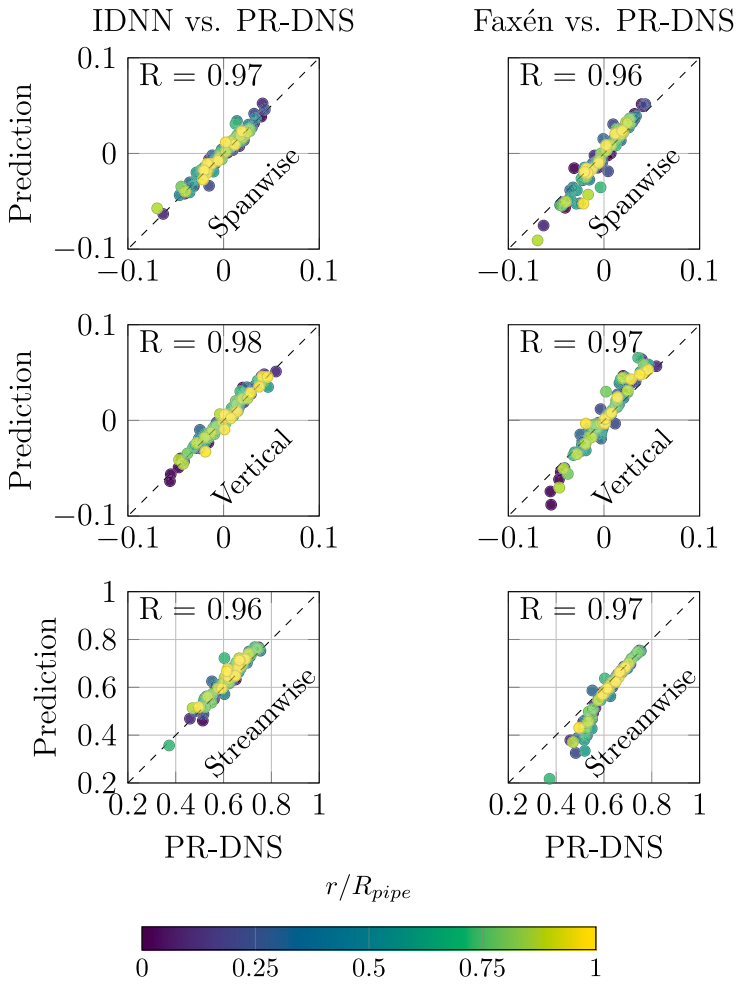


Fig. 10. Comparison between PR-DNS results and both IDNN (left column) and Faxén theory (right column) predictions for each force component, normalized to the theoretical Stokes' force. Each marker is coloured according to its associated relative position in the pipe. The dashed black line indicates a perfect fit.

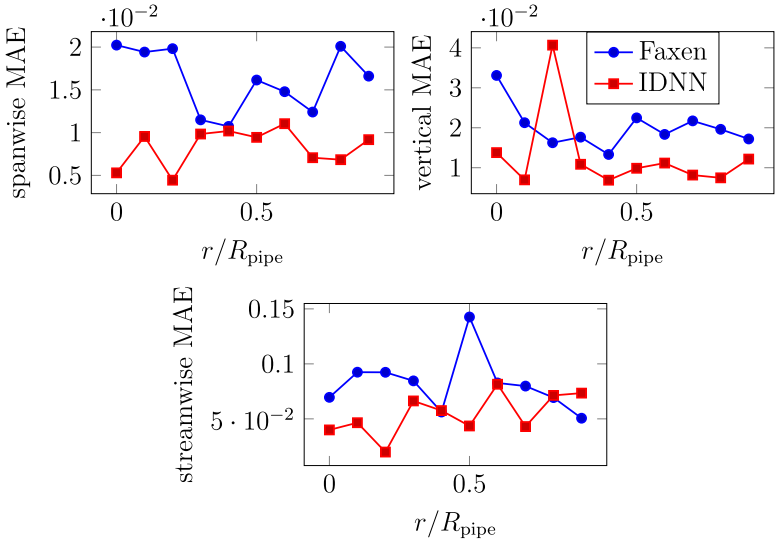


Fig. 11. The Mean Absolute Error (MAE) of the IDNN predictions and the Faxén theory vs. the radial displacement of the particle cloud.

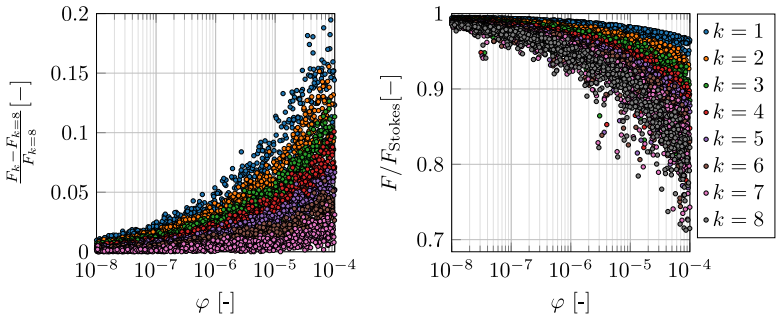


Fig. 12. The error, relative to the case where $k = 8$, at different number of neighbours vs. the volume fraction (left). The predicted force for different number of neighbours vs. the volume fraction (right).

with sparse particle clusters. We compare three approaches: a particle-resolved DNS, Faxén-type predictions that incorporate curvature of the undisturbed flow, and the novel Interaction-Decomposed Neural Network (IDNN) model. The main outcome is that the IDNN reproduces the DNS force components with high correlation across spanwise, vertical, and streamwise drag components, provided the particle cloud remains sufficiently distant from the wall.

To quantify "sufficiently distant", we use Brenner's asymptotic result for wall-normal motion [36]. For a particle of radius $a = d_p/2$ at centre–wall distance δ_w,

$$\frac{F}{6\pi\mu a U} = 1 + \frac{9}{8}\frac{a}{\delta_w} + \mathcal{O}\big((a/\delta_w)^3\big)\,. \tag{16}$$

Requiring the relative correction to remain below a tolerance ϵ yields

$$\frac{\delta_w}{d_p} \geq \frac{9}{16\,\epsilon}. \tag{17}$$

Thus, $\delta_w/d_p \gtrsim 5$ ensures wall effects below 1–2%. For parallel motion, Goldman–Cox–Brenner show a leading correction $\frac{9}{16}(a/\delta_w)$, giving a comparable criterion. Within this regime, the IDNN should consistently outperform the Faxén formulation in predicting the DNS force components.

The parity plots (Fig. 10) show high correlation, $R \gtrapprox 0.96$ between IDNN predictions and DNS across all force components, for both the IDNN and the Faxén model. The streamwise component of the Faxén model appears to show slightly poorer generalization in the area of lower values, where hydrodynamic interactions are more pronounced, while the IDNN performs consistently in the whole range. For the IDNN, 94% of the streamwise predictions fall within the $\pm 1.96\sigma$ confidence interval of the error, corresponding to the expected 95%, while the spanwise and vertical components achieve 96% and 94%, respectively. The error-versus-radius view (Fig. 11) further clarifies the spatial structure of model performance: the IDNN maintains low relative error across radii, with transient degradations near positions where wall effects and neighbour induced interactions compound, whereas Faxén errors rise noticeably, reflecting its limited handling of multi-particle near-field hydrodynamics in confined geometries. These results are aligned with the hypothesis that a neighbour aware surrogate model trained on particle clusters captures dominant interaction modes more faithfully than Laplacian-based corrections.

We identify two reasons to explain such results. First, the IDNN leverages explicit neighbour geometry rather than a volume-fraction based approach. This preserves configuration-level variability that is pronounced even at dilute ϕ. This is evident from the BEM database, as it exhibits widening drag distributions with increasing ϕ while still deep in the dilute regime, underscoring the importance of local arrangement beyond scalar ϕ alone. Second, the DNS simulations were executed with carefully quantified discretization uncertainty, enabling a precise target for learning-based comparison. This reduces the risk of numerical dispersion influencing the results and strengthens confidence in the reported gains of the surrogate.

Despite these strengths, the present modelling approach has clear boundaries of validity. Most notably, it is seen from Fig. 12 that including more neighbours consistently reduces error, indicating that in a real, multi-particle system of many particles, the hydrodynamic influence goes beyond just the five nearest neighbours. Nonetheless, the inclusion of five nearest neighbours captures the majority of the interaction effects and falls below 5% error compared to the $k = 8$ case for almost all volume fractions tested.

Additionally, the model was trained in unbounded Stokes flow and then applied in a shear-dominated, wall-bounded environment. Its success therefore hinges on the particle cloud being sufficiently far from the wall such that confinement effects remain subdominant. When the cloud approaches the wall, omitted physics — most notably shear-rate-dependent corrections and near-wall lubrication interactions — become increasingly important, and the model error correspondingly increases. This behaviour is consistent with the linear, unbounded Stokes assumptions embedded in the training data and further delineates the regime in which reliable extrapolation can be expected.

From an application standpoint, the demonstrated accuracy at low cost make the IDNN a practical choice for closure in Euler–Lagrange simulations of dilute to moderately dilute flows. It avoids the heavy expense of particle-resolved DNS and the numerical sensitivity of Laplacian evaluations required by Faxén-type corrections, while retaining sensitivity to local particle configuration.

CRediT authorship contribution statement

Nejc Vovk: Writing – original draft, Visualization, Validation, Software. **Jakob Kokovnik:** Investigation, Data curation. **Jure Ravnik:** Writing – review & editing, Supervision, Methodology, Funding acquisition, Conceptualization.

Declaration of competing interest

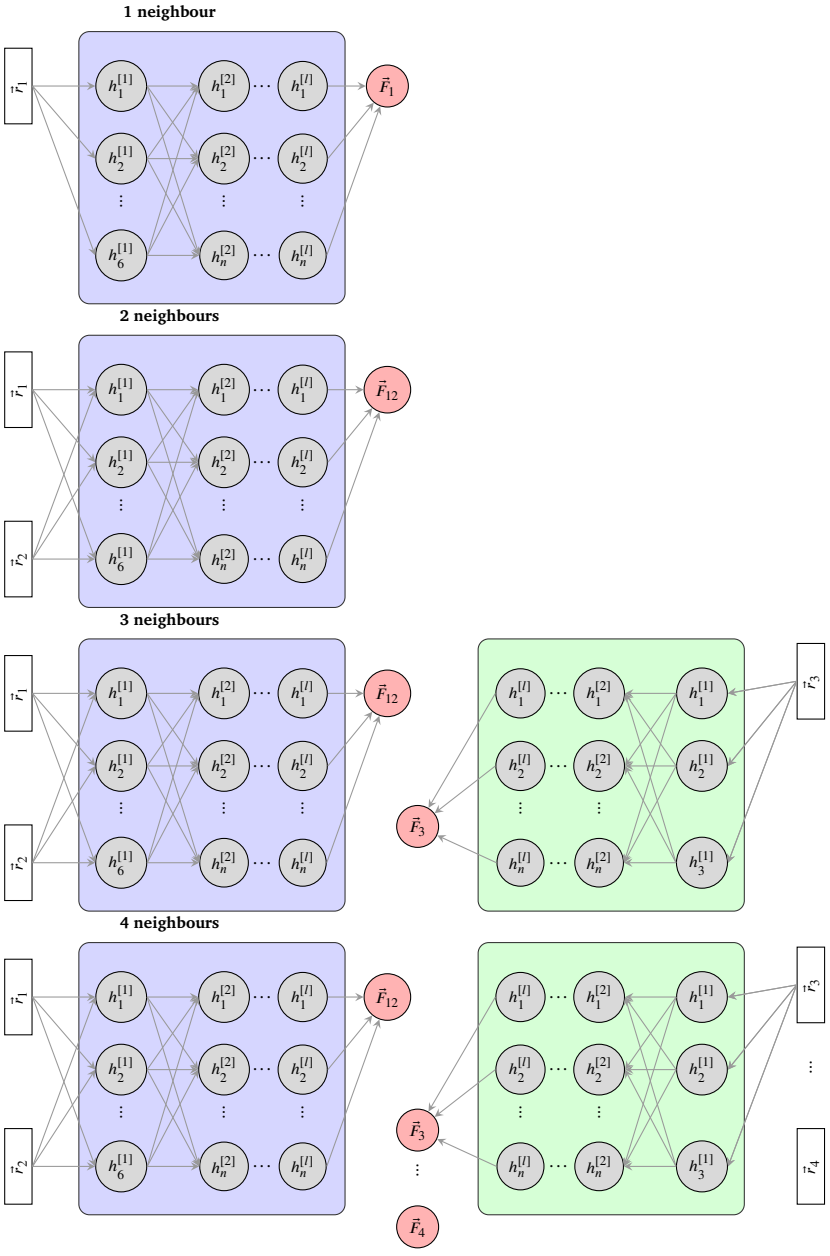
The authors declare that they have no known competing financial interests or personal relationships that could have appeared to influence the work reported in this paper.

Acknowledgements

The authors would like to thank the Slovenian Research and Innovation Agency (research core funding No. P2-0196 and project J7-60118).

Appendix. IDNN architectures for different numbers of neighbours

The following figures show the IDNN architectures for different numbers of neighbours used in the tests discussed in Section 3.4. Only the architectures up to $k = 4$ are shown, as the architectures from there on are the same and the number of inputs increases respectively. For generalization purposes, the number of neurons per layer and the number of layers were kept constant for the second-order block and the first-order blocks; both block consist of three hidden layers with second-order block having 100 neurons per layer and the first-order blocks having 80 neurons per layer. For comparison, only the streamwise force was trained in these tests.



Data availability

Data will be made available on request.

References

[1] C. Marchioli, M. Bourgoin, F. Coletti, R. Fox, J. Magnaudet, M. Reeks, O. Simonin, M. Sommerfeld, F. Toschi, L.P. Wang, S. Balachandar, Particle–laden flows, Int. J. Multiphase Flow 191 (2025) 105291, http://dx.doi.org/10.1016/j.ijmultiphaseflow.2025.105291.

[2] G. Akiki, W. Moore, S. Balachandar, Pairwise-interaction extended point-particle model for particle-laden flows, J. Computational Phys. 351 (2017) 329–357, http://dx.doi.org/10.1016/j.jcp.2017.07.056.

[3] G. Akiki, T.L. Jackson, S. Balachandar, Force variation within arrays of monodisperse spherical particles, Physical Review Fluids 1 (2016) 044202, http://dx.doi.org/10.1103/PhysRevFluids.1.044202.

[4] A.M. Lattanzi, V. Tavanashad, S. Subramaniam, J. Capecelatro, Stochastic model for the hydrodynamic force in Euler–Lagrange simulations of particle-laden flows, Physical Review Fluids 7 (2022) 014301, http://dx.doi.org/10.1103/PhysRevFluids.7.014301.

[5] Y. Xia, Z. Lin, Y. Guo, Z. Yu, Modelling of filtered drag force for clustered particle-laden flows based on interface-resolved simulation data, J. Fluid Mech. 998 (2024) A57, http://dx.doi.org/10.1017/jfm.2024.857.

[6] P. Wang, Y. Lei, Z. Zhu, X. Zheng, Drag model of finite-sized particle in turbulent wall-bound flow over sediment bed, J. Fluid Mech. 964 (2023) A9, http://dx.doi.org/10.1017/jfm.2023.206.

[7] S. Hwang, J. Pan, L.S. Fan, Deep learning for drag force modelling in dilute, poly-dispersed particle-laden flows with irregular-shaped particles, Chemical Engineering Sci. 266 (2023) 118299, http://dx.doi.org/10.1016/j.ces.2022.118299.

[8] T. Tian, H. Zhao, H. Zhang, D. Han, J. Chen, A physics-informed neural network for predicting the drag coefficient of irregular particles utilizing computational fluid dynamics, Phys. Fluids 37 (2025) 073369, http://dx.doi.org/10.1063/5.0279195.

[9] R. Hassanian, A. Helgadóttir, F. Gharibi, A. Beck, M. Riedel, Data-driven deep learning models in particle-laden turbulent flow, Physics Fluids 37 (2025) 023348, http://dx.doi.org/10.1063/5.0251765.

[10] S. Kim, S.J. Karrila, Microhydrodynamics: Principles and Selected Applications; Dover Civil and Mechanical Engineering, Dover Publications, Incorporated, Newburyport, 2005.

[11] Y. Rosenstein, M.L. Alexander, The oseen problem for a finite collection of spheres settling in a viscous liquid, European J. Mechanics – B/Fluids 31 (2012) 71–79, http://dx.doi.org/10.1016/j.euromechflu.2011.08.005.

[12] F. Battista, J.P. Mollicone, P. Gualtieri, R. Messina, C.M. Casciola, Exact regularised point particle (ERPP) method for particle-laden wall-bounded flows in the two-way coupling regime, J. Fluid Mech. 878 (2019) 420–444, http://dx.doi.org/10.1017/jfm.2019.622.

[13] C.D. Dritselis, N.S. Vlachos, Numerical study of educed coherent structures in the near-wall region of a Particle-Laden channel flow, Physics Fluids 20 (2008) 055103, http://dx.doi.org/10.1063/1.2919108.

[14] B. Arcen, A. Tanire, B. Oesterl, On the influence of near-wall forces in particle-laden channel flows, Int. J. Multiphase Flow 32 (2006) 1326–1339, http://dx.doi.org/10.1016/j.ijmultiphaseflow.2006.06.009.

[15] M. Štrakl, M. Hriberšek, J. Wedel, P. Steinmann, J. Ravnik, A Model for Translation and Rotation Resistance Tensors for Superellipsoidal Particles in Stokes Flow, J. Marine Sci. Eng. 10 (2022) 369, http://dx.doi.org/10.3390/jmse10030369.

[16] M. Štrakl, M. Hribersek, J. Wedel, P. Steinmann, J. Ravnik, Superellipsoid force torque model, Zenodo (2022) http://dx.doi.org/10.5281/ZENODO.14824107.

[17] H.G. Weller, G. Tabor, H. Jasak, C. Fureby, A tensorial approach to computational continuum mechanics using object-oriented techniques, Computers Phys. 12 (1998) 620–631, http://dx.doi.org/10.1063/1.168744.

[18] I. Celik, G. Urmila, J.R. Patrick, J.F. Christopher, Procedure for Estimation and Reporting of Uncertainty Due to Discretization in CFD Applications, J. Fluids Eng. 130 (2008) 078001, http://dx.doi.org/10.1115/1.2960953.

[19] J.F. Brady, G. Bossis, Stokesian Dynamics, Annual Review of Fluid Mechanics 20 (1988) 111–157, http://dx.doi.org/10.1146/annurev.fl.20.010188.000551.

[20] B. Felderhof, Many-body hydrodynamic interactions in suspensions, Physica A: Statistical Mechanics its Applications 151 (1988) 1–16, http://dx.doi.org/10.1016/0378-4371(88)90036-2.

[21] P. Mazur, W. Van Saarloos, Many-sphere hydrodynamic interactions and mobilities in a suspension, Physica A: Statistical Mechanics and its Applications 115 (1982) 21–57, http://dx.doi.org/10.1016/0378-4371(82)90127-3.

[22] C.W. Oseen, Ueber die Stokes' sche formel, und iiber eine venvandt. e aufgabe in der hydrodynamik, Ark. Math. Astronom. Fys 6 (1910).

[23] A.M. Fiore, J.W. Swan, Fast Stokesian dynamics, J. Fluid Mech. 878 (2019) 544–597, http://dx.doi.org/10.1017/jfm.2019.640.

[24] K.W. Torre, J. de Graaf, Hydrodynamic Interactions in Particle Suspensions: A Perspective on Stokesian Dynamics, 2025, http://dx.doi.org/10.48550/arXiv.2503.16083, [arXiv:physics/2503.16083].

[25] G. Akiki, T.L. Jackson, S. Balachandar, Pairwise interaction extended point-particle model for a random array of monodisperse spheres, J. Fluid Mech. 813 (2017) 882–928, http://dx.doi.org/10.1017/jfm.2016.877.

[26] A. Seyed-Ahmadi, A. Wachs, Physics-inspired architecture for neural network modeling of forces and torques in particle-laden flows, Computers Fluids 238 (2022) 105379, http://dx.doi.org/10.1016/j.compfluid.2022.105379.

[27] L. Jbara, Z. Cheng, A. Wachs, A physics-inspired neural network to model higher order hydrodynamic interactions in heterogeneous suspensions, Int. J. Multiphase Flow 185 (2025) 105131, http://dx.doi.org/10.1016/j.ijmultiphaseflow.2025.105131.

[28] Ravnik, J. Andromeda, A BEM based Stokes flow solver, Zenodo (2025) http://dx.doi.org/10.5281/ZENODO.14801782.

[29] J. Ravnik, Analytical expressions for singular integrals arising from the 3D Laplace and Stokes Kernels when using constant or linear triangular and quadrilateral boundary elements, Eng. Analys. Boundary Elements 154 (2023) 47–53, http://dx.doi.org/10.1016/j.enganabound.2023.02.057.

[30] P.J. Clark, F.C. Evans, Distance to Nearest Neighbor as a Measure of Spatial Relationships in Populations, Ecology 35 (1954) 445–453, http://dx.doi.org/10.2307/1931034.

[31] M. Štrakl, J. Wedel, P. Steinmann, M. Hriberšek, J. Ravnik, Numerical drag and lift prediction framework for superellipsoidal particles in multiphase flows, Int. J. Comput. Methods Exp. Meas. 10 (2022) 38–49, http://dx.doi.org/10.2495/CMEM-V10-N1-38-49.

[32] A. Paszke, S. Gross, S. Chintala, G. Chanan, E. Yang, Z. DeVito, Z. Lin, A. Desmaison, L. Antiga, A. Lerer, Automatic differentiation in PyTorch, 2017.

[33] H. Faxén, Der Widerstand gegen die Bewegung einer starren Kugel in einer zähen Flüssigkeit, die zwischen zwei parallelen ebenen Wänden eingeschlossen ist, Annalen Physik 373 (1922) 89–119, http://dx.doi.org/10.1002/andp.19223731003.

[34] S. Tenneti, R. Garg, S. Subramaniam, Drag law for monodisperse gas–solid systems using particle-resolved direct numerical simulation of flow past fixed assemblies of spheres, Int. J. Multiphase Flow 37 (2011) 1072–1092, http://dx.doi.org/10.1016/j.ijmultiphaseflow.2011.05.010.

[35] A.A. Zaidi, T. Tsuji, T. Tanaka, A new relation of drag force for high Stokes number monodisperse spheres by direct numerical simulation, Advanced Powder Tech. 25 (2014) 1860–1871, http://dx.doi.org/10.1016/j.apt.2014.07.019.

[36] H. Brenner, The slow motion of a sphere through a viscous fluid towards a plane surface, Chem. Eng. Sci. 16 (3–4) (1961) 242–251.